Available online at www.sciencedirect.com
ScienceDirect
Catalysis Today 139 (2009) 312–321
CATALYSIS TODAY
www.elsevier.com/locate/cattod

Steady-state and dynamic modeling of indirect partial oxidation of methane in a wall-coated microchannel

Mustafa Karakaya, Ahmet K. Avcı *, A. Erhan Aksoylu, Z. İlsen Önsan

Department of Chemical Engineering, Boğaziçi University, Bebek 34342, Istanbul, Turkey

Available online 2 April 2008

Abstract

Steady and dynamic characteristics of catalytic indirect partial oxidation (combined total oxidation and steam reforming) of methane to hydrogen in a wall-coated microchannel are investigated using computational techniques. Steady-state behavior is initially modeled using a two-dimensional axisymmetrical wall-coated reactor model. Considering the small channel diameter, adiabatic operation and negligible transport resistances, response of the microchannel is also investigated using a one-dimensional pseudohomogeneous tubular reactor model. Simulations of the microchannel are carried out using both models for different feed conditions ranging between 1.89 and 2.24 for CH_4/O_2 and 1.17–2.34 for H_2O/CH_4. Outcomes from both models are found to be close, allowing the use of the low-cost one-dimensional model in dynamic simulations. Analysis of transients during the system start-up indicate that steady state is reached between 100 and 120 s depending on the feed composition. Product temperature and flow rates obtained from steady-state and dynamic simulations are found to be close with some differences arising from the finite difference-based numerical method used to solve partial differential equations of the dynamic model. Dynamic responses of the microchannel to several disturbances in the feed are analyzed. The response to a step increase in the inlet oxygen flow rate (decrease of CH_4/O_2 from 2.24 to 1.89) is the elevation of temperature by ca. 100 K, which in turn leads to ca. 33% in hydrogen yield, and the time to reach the new steady state is around 90 s. If the disturbance involves an increase in inlet steam flow, temperature and hydrogen yield decrease in time to a local minimum within 10 s and then gradually increase to the subsequent steady state within 50 s ending up with net reductions of ca. 1.6% and 9%, respectively.

Keywords: Modeling; Dynamic response; Microchannel; Hydrogen production; Partial oxidation; Methane

1. Introduction

Fuel cells have been recognized to have significant advantages over their conventional counterparts, such as the internal combustion engine (ICE), in clean and efficient power generation [1,2]. Zero emission can be achieved if pure hydrogen is used as the fuel. Apart from their potential use in powering vehicles, fuel cells find widespread use in stationary applications, ranging from small systems located in remote areas and residences in urban areas to large central power stations [3,4].

The alternative to establishing a hydrogen refueling infrastructure that complies with mobile or stationary applications is to carry or store readily available fuels (primary fuels) that have high-energy densities and to convert them to a hydrogen-rich gas via a fuel processor, on an as-needed basis [5,6]. The fuel processor, which now becomes a part of the fuel cell engine (fuel processor/fuel cell assembly), must also meet the requirements of size and weight, be able to start up very quickly, and be dynamically responsive to changing power demands, which impose a varying fuel processing rate [2]. The fuel processor/fuel cell assembly is an integrated system consisting of several reactors, heat exchangers, evaporators, a control unit, peripherals and finally the fuel cell [7,8].

One route for production of fuel-cell grade hydrogen is indirect partial oxidation of methane (IPOX), which is basically a combination of total oxidation (TOX) (Reaction (1)) of part of the primary fuel and the simultaneous or subsequent steam reforming (SR) (Reaction (2)) of the remaining, running together with the water-gas shift (WGS) reaction (Reaction (3)) [6–9]:

$$CH_4 + 2O_2 = CO_2 + 2H_2O, \quad \Delta H^{\circ}_{298} = -802.3\,\mathrm{kJ/(g\,mol)} \tag{1}$$

* Corresponding author. Tel.: +90 212 3597785; fax: +90 212 2872460.
E-mail address: avciahme@boun.edu.tr (A.K. Avcı).

0920-5861/$ – see front matter © 2008 Elsevier B.V. All rights reserved.
doi:10.1016/j.cattod.2008.02.015

Nomenclature

a_c	total surface area of catalyst per unit mass (m^2 kg-cat^{-1})
A_c	cross-sectional area of reactor (m^2)
c_j	concentration of species j (kmol m^{-3})
c_{pj}	heat capacity of species j (kJ kmol^{-1} K^{-1})
D_{er}	effective radial diffusivity of gas mixture (m^2 s^{-1})
E_i	activation energy of reaction i (kJ kmol^{-1})
F_j	flow rate of species j (kmol s^{-1})
F_{j0}	flow rate of species j at $t = 0$ (kmol s^{-1})
F_j^{in}	flow rate of species j at $z = 0$ (kmol s^{-1})
F_T	total flow rate (kmol s^{-1})
F_T^{in}	total flow rate at $z = 0$ (kmol s^{-1})
GHSV	gas hourly space velocity (m^3-gas m^3-reactor^{-1} h^{-1})
ΔH_i	heat of reaction i at T (kJ g mol^{-1})
$\Delta H^c_{CH_4}$	heat of adsorption of methane (kJ kmol^{-1})
$\Delta H^c_{O_2}$	heat of adsorption of oxygen (kJ kmol^{-1})
i	reaction index
j	species index
k_i	rate constant for reaction i (kmol kg-cat^{-1} h^{-1})
k_{0i}	intrinsic reaction rate of reaction i (kmol kg-cat^{-1} h^{-1})
$K_{eq,i}$	equilibrium constant of reaction i, (bar^2 for $i = 2$, dimensionless for $i = 3$)
$K^c_{CH_4}$	adsorption equilibrium constant for methane (bar^{-1})
$K^c_{CH_4,0}$	pre-exponential factor used for calculating $K^c_{CH_4}$ (bar^{-1})
$K^c_{O_2}$	adsorption equilibrium constant for oxygen (bar^{-1})
$K^c_{O_2,0}$	pre-exponential factor used for calculating $K^c_{O_2}$ (bar^{-1})
L	length of the microchannel (m)
p_j	partial pressure of species j (bar)
p_T	total pressure (bar)
p_T^{in}	total pressure at $z = 0$ (bar)
$-r_i$	rate of reaction i (kmol kg-cat^{-1} s^{-1})
R_j	total rate of formation or depletion of species j (kmol kg-cat^{-1} s^{-1})
Re	Reynolds number
t	time (s)
T	temperature (K)
T_{exit}	reactor exit temperature at steady state (K)
T_0	temperature at $t = 0$ (K)
T^{in}	temperature at $z = 0$ (K)
u_{max}	linear fluid velocity at the centerline ($\xi = 0$) (m s^{-1})
v	volumetric flow rate (m^3 s^{-1})
v^{in}	inlet volumetric flow rate (m^3 s^{-1})
x_{CH_4}	methane conversion at steady state
y_{CO}	carbon monoxide yield at steady state (moles of CO produced/100 moles of CH_4 fed)
y_{H_2}	hydrogen yield at steady state (moles of H_2 produced/100 moles of CH_4 fed)
z	axial coordinate (m)

Greek letters

ε_{bed}	bed void fraction
λ_{er}	effective radial thermal conductivity of gas mixture (W m^{-1} K^{-1})
ξ	radial coordinate (m)
ρ_b	bulk catalyst density (kg-cat m^{-3})
ϕ	diameter of the microchannel (m)

$$CH_4 + H_2O = CO + 3H_2, \quad \Delta H^\circ_{298} = 206.2\,\text{kJ/(g mol)} \qquad (2)$$

$$CO + H_2O = CO_2 + H_2, \quad \Delta H^\circ_{298} = -41.2\,\text{kJ/(g mol)} \qquad (3)$$

Reforming of CO_2 runs much slower than Reaction (2) in the presence of sufficient steam, and, its existence is therefore neglected [6]. The IPOX reactor lies at the heart of a fuel processor/fuel cell assembly for use in mobile or small-scale stationary applications; it is the main hydrogen-generating unit which is followed by hydrogen enriching and cleaning units, i.e. water-gas shift and preferential CO oxidation (PROX) reactors [7,8]. The success of the IPOX route depends on the degree of heat transfer achieved between exothermic TOX and endothermic SR reactions. This can be achieved on a nanoscale basis by using a bimetallic Pt–Ni catalyst on which Pt and Ni metals are reported to help in driving total oxidation and steam reforming of light hydrocarbons, respectively, thus making the catalyst to act like a heat exchanger [10,11]. In addition to the heat transfer between the two reactions, transport resistances between the bulk fluid and solid catalyst phases can also be significant due to the presence of high reaction enthalpies (-802.3 kJ mol^{-1} for TOX and 206.2 kJ mol^{-1} for SR). At this point, reactor geometry, in addition to the type of catalyst, can be critical: the use of microstructured multichannel wall-coated catalytic microreactors can improve the IPOX performance. Micrometer-scale characteristic dimensions of the microchannel reactors facilitate heat transfer between the two reactions (Reactions (1) and (2)) and minimize heat and mass transfer resistances [12–15]. These novel reactors are compact and have high surface area-to-volume ratios that help in resolving the volumetric space related issues and improving dynamic response characteristics against changes in the feed conditions. These beneficial features make microchannel reactors ideal for use as fuel processors in hydrogen fuel cell applications [12–15].

The fuel processor/fuel cell assembly can be modeled accurately for steady-state operation, but analysis of transient response to a rapid change in the operating conditions (such as feed composition) in stationary or mobile applications calls for the development of a dynamic model [2]. It can then be possible to implement accurate control and coordination of the assembly based on its dynamic behavior. In multichannel wall-coated microreactors, analysis of a single channel can represent the

behavior of the whole reactor, since the channels have identical geometries and are subject to the same operating conditions [15]. It is reported that the diffusion paths in catalytic coatings of the microchannels are small, so that heat and mass transport resistances can be neglected [15,16]. In addition, small channel diameters and presence of adiabatic conditions allow neglection of gradients in the radial direction. Therefore the catalytic phenomena occurring at the channel walls can be considered to run within a pseudohomogeneous tubular geometry at a single spatial dimension, which can be modeled using a one-dimensional pseudohomogeneous tubular reactor model [16].

The present paper investigates steady-state and dynamic behaviors of indirect partial oxidation of methane to hydrogen over a bimetallic Pt–Ni/δ-Al_2O_3 catalyst coated on the walls of a microchannel operating adiabatically. For this purpose a two-dimensional axisymmetric wall-coated reactor model is formulated. This model is then compared with a one-dimensional pseudohomogeneous tubular reactor model to verify the statements mentioned above. Comparisons are made at steady state for a set of feed conditions (CH_4/O_2 = 1.89–2.24 and H_2O/CH_4 = 1.17–2.34) and the results from both models are found to give similar results (Section 4) which allows the use of a one-dimensional model through which the transient behavior of the microchannel is much easier to formulate and faster to solve. Therefore, the one-dimensional model is used to study the start-up phenomena within the catalytic microchannel for different feed compositions. In addition to start-up characterization, responses of the microchannel, which is initially at steady state, to a set of disturbances in the feed, i.e. changes in methane-to-oxygen and steam-to-methane ratios, are analyzed. Parameters that quantify the dynamics of the reaction system such as qualitative and quantitative variations in product flow rates and the time to reach to new steady states are figured out.

2. Mathematical modeling

Methane can be converted to hydrogen over a bimetallic Pt–Ni catalyst by indirect partial oxidation which is the combination of total oxidation, steam reforming and WGS reactions (Reactions (1)–(3), respectively) [10]. This process is autothermal, i.e. heat and part of the steam released by exothermic total oxidation, driven mainly by the Pt sites, are harnessed by endothermic steam reforming, driven mainly by the Ni sites [10,11]. The first step in indirect partial oxidation is the initiation of catalytic combustion, also called surface ignition (Reaction (1)). Once triggered, the process involving oxidation and steam reforming sustains itself. However, the light-off temperature at which ignition takes place depends on the type of fuel being used and the inlet fuel/oxygen ratio. The light-off temperature is defined as the value at which 10% of the oxidation conversion of the fuel is obtained [10,17].

2.1. Steady-state operation

The steady-state behavior of the wall-coated microchannel having a circular cross-section can be modeled using a two-dimensional axisymmetric reactor model. In this model (Eqs. (4)–(10)), reactions run on the catalytic wall of the microchannel, the thickness of the catalyst layer is neglected and adiabatic operating conditions are assumed:

$$u_{\max}\left[1-\left(\frac{2\xi}{\phi}\right)^2\right]\frac{\partial c_j}{\partial z}=D_{\mathrm{er}}\left[\frac{1}{\xi}\frac{\partial c_j}{\partial \xi}+\frac{\partial^2 c_j}{\partial \xi^2}\right] \tag{4}$$

$$u_{\max}\left[1-\left(\frac{2\xi}{\phi}\right)^2\right]\rho_g c_p\frac{\partial T}{\partial z}=\lambda_{\mathrm{er}}\left[\frac{1}{\xi}\frac{\partial T}{\partial \xi}+\frac{\partial^2 T}{\partial \xi^2}\right] \tag{5}$$

$$\frac{\partial c_j}{\partial \xi}=0 \quad (\text{at } \xi=0) \tag{6}$$

$$\frac{\partial T}{\partial \xi}=0 \quad (\text{at } \xi=0) \tag{7}$$

$$-D_{\mathrm{er}}\frac{\partial c_j}{\partial \xi}=\frac{R_j}{a_c} \quad (\text{at } \xi=\phi/2) \tag{8}$$

$$-\lambda_{\mathrm{er}}\frac{\partial T}{\partial \xi}=\frac{\sum_{i=1}^{3}(-\Delta H_i)(-r_i)}{a_c} \quad (\text{at } \xi=\phi/2) \tag{9}$$

$$F_j=F_j^{\mathrm{in}};\qquad T=T^{\mathrm{in}} \quad (\text{at } z=0) \tag{10}$$

In Eqs. (4)–(10), i and j are reaction and component indexes, respectively. Total number of reactions and components involved in methane IPOX are taken as 3 (TOX, SR and WGS) and 7 (CH_4, H_2O, CO, CO_2, H_2, O_2 and N_2), respectively.

It has been reported that microchannel reactors are employed in measuring intrinsic rate constants of heterogeneously catalyzed reactions [15,16]. This is due to the fact that heat and mass transfer resistances are negligible as a result of micro-scale characteristic dimensions and short diffusion paths [15]. Neglection of transport resistances allows the reaction system to behave like a pseudohomogeneous entity. In addition, radial gradients can be ignored due to the small channel diameters and adiabatic conditions employed. Therefore, the behavior of the wall-coated microchannel can also be quantified by using a one-dimensional pseudohomogeneous tubular reactor model (Eqs. (11)–(13)):

$$\frac{\mathrm{d}F_j}{\mathrm{d}z}=A_c\rho_b R_j \tag{11}$$

$$\frac{\mathrm{d}T}{\mathrm{d}z}=\frac{A_c\rho_b\sum_{i=1}^{3}(-\Delta H_i)(-r_i)}{\sum_{j=1}^{7}F_j c_{pj}} \tag{12}$$

$$F_j=F_j^{\mathrm{in}};\qquad T=T^{\mathrm{in}} \quad (\text{at } z=0) \tag{13}$$

Rate laws of IPOX reactions (Reactions (1)–(3)) are obtained from literature. Total oxidation of methane (Reaction (1)) is reported to be driven mainly by the Pt metal of the bimetallic Pt–Ni/δ-Al_2O_3 catalyst [11]. Therefore, the rate of TOX is calculated using the Langmuir–Hinshelwood type expression proposed by Ma et al. [17] for a Pt/δ-Al_2O_3 catalyst:

$$-r_1=\frac{k_1 K^c_{CH_4}p_{CH_4}\sqrt{K^c_{O_2}p_{O_2}}}{\left(1+K^c_{CH_4}p_{CH_4}+\sqrt{K^c_{O_2}p_{O_2}}\right)^2} \tag{14}$$

Table 1
Parameters for calculation of the rate and adsorption equilibrium constants in Eq. (14) [17]

	k_{01} (kmol kg-cat^{-1} h^{-1})	E_1 (kJ kmol^{-1})
$k_1 = k_{01}\exp\left(-\frac{E_1}{RT}\right)$	135.587	−34,153
	$K^{c}_{CH_4,0}$ (bar^{-1})	$\Delta H^{c}_{CH_4}$ (kJ kmol^{-1})
$K^{c}_{CH_4} = K^{c}_{CH_4,0}\exp\left(-\frac{\Delta H^{c}_{CH_4}}{RT}\right)$	3×10^{17}	−231,680
	$K^{c}_{O_2,0}$ (bar^{-1})	$\Delta H^{c}_{O_2}$ (kJ kmol^{-1})
$K^{c}_{O_2} = K^{c}_{O_2,0}\exp\left(-\frac{\Delta H^{c}_{O_2}}{RT}\right)$	2×10^{23}	−306,191

Temperature dependence of the rate and adsorption equilibrium constants of Eq. (14) are expressed by equations of the Arrhenius type whose parameters are given in Table 1.

Methane steam reforming and the accompanying water-gas shift reactions are found to be catalyzed mainly by the Ni sites of the bimetallic catalyst [11]. Based on this fact, kinetic expressions proposed by Numaguchi and Kikuchi [18] for calculating rates of methane SR (Eq. (15)) and WGS (Eq. (16)) over a Ni/Al_2O_3 catalyst are used, and the parameters of these equations are given in Table 2:

$$-r_2 = \frac{k_2(p_{CH_4} - p^3_{H_2}p_{CO}/K_{eq,2})}{p^{0.596}_{H_2O}} \tag{15}$$

$$-r_3 = k_3\left(p_{CO} - \frac{p_{H_2}p_{CO_2}}{K_{eq,3}}\right) \tag{16}$$

2.2. Dynamic operation

The equations for the steady-state models also hold for the dynamic models with the addition of the time-dependent concentration and temperature terms which lead to a system of partial differential equations (PDE) as in the case of one-dimensional pseudohomogeneous model (Eqs. (17)–(20)):

$$\varepsilon_{bed}\frac{\partial c_j}{\partial t} = -\frac{1}{A_c}\frac{\partial F_j}{\partial z} + \rho_b R_j \tag{17}$$

$$\varepsilon_{bed}\sum_{j=1}^{7}(c_j c_{pj})\frac{\partial T}{\partial t} = -\frac{\sum_{j=1}^{7}(F_j c_{pj})}{A_c}\frac{\partial T}{\partial z} + \rho_b\sum_{i=1}^{3}(-\Delta H_i)(-r_i) \tag{18}$$

$$F_j = F_{j0}; \qquad T = T_0 \quad (\text{at } t = 0) \tag{19}$$

$$F_j = F^{in}_j; \qquad T = T^{in} \quad (\text{at } z = 0) \tag{20}$$

The variables and their units in Eqs. (17)–(20) are the same as those for the steady-state model (Eqs. (11)–(13)).

Effect of volume change in gas phase is usually neglected when the difference between the amounts of reactants and products is small. However, Reaction (2) reveals that volume change needs to be included in the model since 3 moles of hydrogen are produced from 1 mole of methane. The steady-state model captures this effect implicitly while an extra equation is necessary in the dynamic model. This arises from the relation $F_j = c_j v$, which is used for conversion from concentration to flow rate in Eqs. (17) and (18) during the simulation. Volume change with reaction is evaluated using the following relation:

$$v = v^{in}\left(\frac{F_T}{F^{in}_T}\right)\frac{p^{in}_T}{p_T}\left(\frac{T}{T^{in}}\right) \tag{21}$$

where v is the volumetric flow rate anywhere in the reactor at any time, F_T and T the total flow rate and temperature anywhere in the bed at any time. Differentiating Eq. (21) with respect to the spatial coordinate z and neglecting pressure drop, one obtains

$$\frac{dv}{dz} = \frac{v^{in}}{F^{in}_T T^{in}}\left(T\frac{dF_T}{dz} + F_T\frac{dT}{dz}\right) \tag{22}$$

The time dependence of v is handled implicitly through the dependence of F_T and T by Eqs. (17) and (18) with which Eq. (22) is coupled at each time step.

2.3. Numerical methods

In solving the two-dimensional axisymmetric wall-coated reactor model (Eqs. (4)–(10)), which are partial differential in character, the first and second derivatives of concentration (c_j) and temperature (T) with respect to radius (ξ) are approximated using a forward finite difference formula and a second order central difference formula, respectively, by dividing the radial domain into 50 equal intervals. The resulting ordinary differential equations are then solved along the axial direction using the method of lines.

The differential mole and energy balances comprising the steady-state one-dimensional pseudohomogeneous tubular reactor model (Eqs. (11)–(13)) form a system of ordinary differential equations (ODE). This equation set is solved using a modified Runge–Kutta routine capable of handling stiff systems under the MATLAB™ environment.

The system of coupled non-linear partial differential equations ((17)–(20)), describing the transient (dynamic)

Table 2
Rate equations for methane steam reforming and water-gas shift reactions

i	k_{0i} [a] (g mol kg-cat^{-1} s^{-1})	E_i [a] (kJ kmol^{-1})	$K_{eq,i}$	Reference
2	2.62×10^5 bar$^{-0.404}$	106,900	$4.707 \times 10^{12}\exp(-224{,}000/(RT))$ bar^2	[18]
3	2.45×10^2 bar^{-1}	54,500	$1.142 \times 10^{-2}\exp(-37{,}300/(RT))$	

[a] $k_i = k_{0i}\exp(-E_i/RT)$.

one-dimensional pseudohomogeneous tubular reactor model, are discretized both in the spatial and temporal domains using the explicit, finite difference-based two-step Lax–Wendroff method, whose stability is controlled by the Courant–Friedrichs–Levy (CFL) criterion [19,20]. In this method, the spatial domain is divided into 50 equal increments and a time step in the order of 10^{-4} s is used to ensure preventing non-physical oscillations of the time-dependent and position-dependent variables. The CPU time is accordingly high, which varies between 10 and 13 h for one single simulation on a Hewlett-Packard workstation xw6200 equipped with a Pentium 4 Xeon processor running at 2.8 GHz. A computer code comprised of several subroutines for evaluation of the reaction rates, heat capacities and heat of reactions is compiled and executed under the MATLAB^{TM} environment.

2.4. Operating conditions

The operating conditions and geometric data used in the steady-state and dynamic simulations are given in Table 3. Operating conditions and data pertinent only to dynamic simulations are presented separately in Tables 4 and 5. The amount of methane fed is kept constant in each run and air and steam flow rates at the reactor inlet are dictated by the methane-to-oxygen (CH_4/O_2) and steam-to-methane (H_2O/CH_4) ratios. Data given in Table 3 are adapted from the data of an experimental autothermal steam reforming reactor reported by Ma and Trimm [10]. Note that data such as ρ_b and ε_{bed} are used only in simulating the microchannel behavior using the one-dimensional model based on the reasons mentioned in Section 2.1 and discussed in Section 3.

Apart from CH_4/O_2 and H_2O/CH_4 ratios, another operating parameter is the gas hourly space velocity (GHSV) defined as the amount of gas flowing in the channel (m^3 gas m^3 reactor^{-1} h^{-1}) at standard temperature and pressure. The amount of methane fed into the channel is kept constant in each run by adjusting the GHSV values accordingly [10]. In all runs, the feed mixture is composed of methane, air and steam.

Table 3
Operating conditions and geometric data

T^{in} (K)	800
$F^{in}_{CH_4}$ (kmol s^{-1})	4.65×10^{-8}
p^{in}_T (atm)	2.9
ϕ (m)	1.3×10^{-3}
L (m)	3.2×10^{-1}
a_c (m^2 kg-cat^{-1})	1.07×10^{5}
λ_{er} (W m^{-1} K^{-1})	2.2×10^{-1}
D_{er} (m^2 s^{-1})	4.25×10^{-5}
ρ_b (kg m^{-3})	1167
ε_{bed}	0.45

When considering dynamic simulations, particular emphasis should be made that start-up of the reactor and start-up of indirect partial oxidation are considered as two different phenomena. In the case of reactor start-up, there is no flow in the reactor initially. At $t = 0$, flow of a non-reactive gas, nitrogen, is allowed at a predetermined rate, the dynamics of which is governed solely by the laws of fluid dynamics. Once the flow rate and temperature settle to a steady-state value, the reactive mixture consisting of methane, air and steam is fed into the reactor. This is called the start-up of indirect partial oxidation. For simplicity, it is assumed that the non-reactive nitrogen is flowing at the same GHSV and temperature as the reactive gas mixture.

In order to gain insight into the dynamic behavior of the reaction system upon imposition of a change in the feed conditions, two cases are investigated: The first one involves a decrease in the CH_4/O_2 molar ratio, and the second, an increase in the ratio of H_2O/CH_4. The volumetric flow rate is accordingly adjusted so as to keep the amount of methane fed constant at 4.65×10^{-8} kmol s^{-1} before and after the disturbance. The steady-state (or initial) values at $t = 0$ are directly taken from the simulation results for the start-up

Table 4
Initial and feed conditions for the simulation of reactor start-up

Run	$t = 0$, non-reactive flow (N_2)				$t > 0$, reactive flow (CH_4, H_2O and O_2)			
	CH_4/O_2 (mol/mol)	H_2O/CH_4 (mol/mol)	GHSV (h^{-1})	T^{in} (K)	CH_4/O_2 (mol/mol)	H_2O/CH_4 (mol/mol)	GHSV (h^{-1})	T^{in} (K)
1	–	–	37,600	800	2.24	1.17	37,600	800
2	–	–	41,100	800	1.89	1.17	41,100	800
3	–	–	51,300	800	1.89	2.34	51,300	800

Table 5
Feed conditions before and after the disturbance

Case	Before disturbance				After disturbance			
	CH_4/O_2 (mol/mol)	H_2O/CH_4 (mol/mol)	GHSV (h^{-1})	T^{in} (K)	CH_4/O_2 (mol/mol)	H_2O/CH_4 (mol/mol)	GHSV (h^{-1})	T^{in} (K)
1	2.24	1.17	37,600	800	1.89	1.17	41,100	800
2	1.89	1.17	41,100	800	1.89	1.56	44,500	800

Table 6
Comparison of steady-state simulation results from two-dimensional axisymmetrical wall-coated microchannel model (2D WC) and one-dimensional pseudohomogeneous tubular reactor model (1D PH)

Run	Feed conditions			x_{CH_4}			y_{H_2}			y_{CO}			T_{max} (K)		
	CH_4/O_2 (mol/mol)	H_2O/CH_4 (mol/mol)	GHSV (h^{-1})	1D PH	2D WC		1D PH	2D WC		1D PH	2D WC		1D PH	2D WC	
					$\xi = 0$	$\xi = \phi/2$		$\xi = 0$	$\xi = \phi/2$		$\xi = 0$	$\xi = \phi/2$		$\xi = 0$	$\xi = \phi/2$
1	2.24	1.17	37,600	86.83	72.50	74.87	171.25	126.10	130.61	86.80	78.66	79.03	988.10	971.33	970.25
2	1.89	1.17	41,100	96.59	78.91	79.45	184.00	151.83	153.37	96.54	86.25	88.63	1063.55	1051.07	1048.37
3	1.89	2.34	51,300	90.80	73.22	75.51	166.64	132.61	135.08	90.74	79.64	81.00	1054.88	1029.20	1027.80

analysis. The inlet temperatures are not altered. For each case the feed conditions are shown in Table 5.

3. Results and discussion

The steady-state simulation results – total methane conversion, hydrogen and carbon monoxide yields at the reactor exit and maximum temperature in the reactor under the specified feed conditions – from two-dimensional axisymmetric wall-coated reactor model and one-dimensional pseudohomogeneous tubular reactor model are presented in Table 6.

For all feed conditions (Runs 1, 2 and 3 in Table 6), methane conversion and product yields are found to be slightly higher in the catalytic wall ($\xi = \phi/2$) than in the centerline ($\xi = 0$). This is due to the fact that IPOX reactions (Reactions (1)–(3)) are assumed to run in the catalytic zone and homogeneous gas phase reactions are neglected. On the other hand, an opposite trend, i.e. higher T at $\xi = 0$ is observed for the maximum bed temperature, T_{max}. This can be explained by the dominance of endothermic steam reforming at the downstream of the microchannel (shown by a flattening temperature profile towards the exit zone) at which the maximum temperature is observed (Fig. 1). Such an effect can facilitate rate of heat removal within the catalytic zone faster at the microchannel exit due to the dominance of endothermic chemistry, which then causes catalytic wall to become slightly cooler than the gaseous bulk fluid phase.

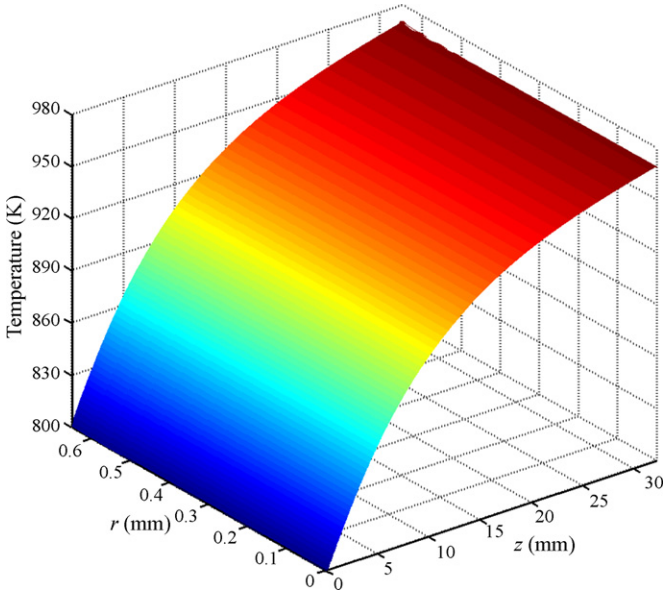

Fig. 1. Axial and radial temperature profiles within the wall-coated microchannel simulated by the two-dimensional axisymmetrical model ($CH_4/O_2 = 2.24$ and $H_2O/CH_4 = 1.17$).

It was mentioned in Section 2.1 that the thickness of the catalyst layer was assumed to be negligible when compared with the microchannel diameter. This causes the dimensions of diffusion paths to be short and, as a result, heat and mass transfer resistances within the catalyst layer to be insignificant, which is one of the beneficial characteristics of the catalytic microstructured reactors [12–15]. Similarly, gradients between the solid and gas phases seem to be negligible. Table 6 demonstrates that the results found at the centerline ($\xi = 0$) and at the catalytic wall ($\xi = \phi/2$) of the microchannel are close to each other. This can be explained by the high fluid flow rates employed (900–1250 cm s^{-1}, corresponding to GHSV values ranging between 37,600 and 51,300 h^{-1}). Presence of such high flow rates helps in minimizing heat and mass transfer resistances between the catalytic wall and the bulk fluid due to a well-mixed environment at the interface. When this fact is combined with the presence of short radial distances and adiabatic operating conditions, temperature and concentration gradients along the radial direction, between the catalytic wall and the gaseous fluid phase, become insignificant (Table 6). It is worth noting that high fluid flow rates given above correspond to Reynolds numbers varying between 160 and 220 due to the small channel diameter employed, 1.3×10^{-3} m (Table 3). This operating window is defined by laminar flow ($Re < 2000$), which is the fluid mechanical characteristic of the microchannel reactors [12–15].

The results above allow the reaction system to be analyzed in one dimension, along the axial coordinate only, and as a pseudohomogeneous entity. Therefore, the steady-state behavior of the microchannel is modeled and simulated using a one-dimensional pseudohomogeneous tubular reactor model (Eqs. (11)–(13)). Outcomes of this model are presented in Table 6 and in Fig. 2. Both models demonstrate similar qualitative responses against changes in the feed ratios. At constant steam-to-methane molar ratio, a decrease in the methane-to-oxygen molar ratio leads to elevated maximum bed temperatures and an increase in the hydrogen yield. Increasing the molar flow rate of oxygen in the feed will result in combustion of more methane; hence more heat will be released

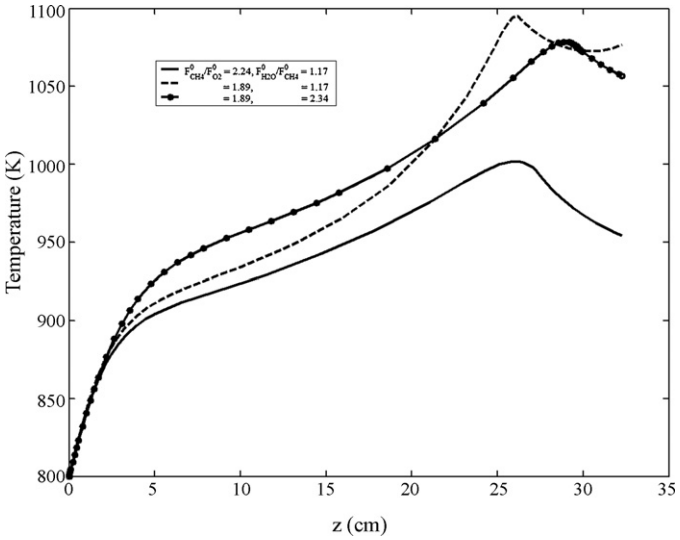

Fig. 2. Axial temperature profiles along the wall-coated microchannel simulated by the one-dimensional tubular reactor model for different feed ratios.

by total oxidation (Fig. 2). Although this will leave less methane for hydrogen generation via Reaction (2), resulting higher bed temperatures will enhance endothermic steam reforming reactions and result in higher hydrogen and carbon monoxide yields, as shown in Table 6 and by Ma and Trimm experimentally [10]. At constant methane-to-oxygen ratio, an increase in the inlet molar flow rate of steam lowers the maximum bed temperature (Table 6 and Fig. 2). A possible explanation is the role of steam in facilitating heat exchange between the Pt and Ni sites on the catalyst, which was demonstrated experimentally for indirect partial oxidation of methane [10] and propane [21]. In most studies, steam is reported to inhibit methane steam reforming, though a few studies indicate zero and positive reaction orders with respect to steam [22]. In parallel to this trend, steam reforming rate law given in Eq. (15) predicts an inverse proportionality between reaction rate and partial pressure of steam [18]. Therefore CO and H_2 yields are found to decrease with an increase in steam flow rate (Table 6).

Comparison of both models on a quantitative basis shows that for all feed ratios, maximum bed temperatures simulated by the one-dimensional model are slightly higher than those estimated by the two-dimensional model, with a difference of ca. 2% or 20 K (Table 6). These differences are based on the average of individual differences between two models calculated for each run (for two-dimensional model, the results reported for the catalytic wall are taken into account). Such a temperature difference can considerably favor kinetics of methane steam reforming at an exponential rate as given in Eq. (15) and in Table 2, which explains the average differences of 10% and 25% in simulated carbon monoxide and hydrogen yields, respectively (Table 6). The ratio of these differences between product yields is equal to 2.5 and is close to the stoichiometric H_2/CO ratio of methane steam reforming (equal to 3); the difference comes mainly from the water-gas shift (Reaction (3)) which runs together with steam reforming and, therefore, consumes hydrogen, back produces carbon monoxide and reduces H_2/CO ratio at high steam reforming conversions (Table 6). This indicates that the deviations between the models are characterized mainly by the temperature sensitivity of methane steam reforming whose magnitude is dictated by the rate expression used (Eq. (15)).

Comparison of the temperature profiles show that the one-dimensional model predicts a hot-spot formation at the downstream zone, followed by a ca. 50 K decrease in temperature, whereas the two-dimensional model predicts a temperature profile flattening smoothly without any hot-spot generation (Figs. 1 and 2, $CH_4/O_2 = 2.24$ and $H_2O/CH_4 = 1.17$). Although both models differ in temperature only by 2%, the difference in the temperature profiles gives an insight about the operation of a wall-coated microchannel reactor and a tubular packed-bed microreactor. The former has much better heat transfer characteristics and temperature can be distributed uniformly along the microchannel, especially when metallic substrates are employed [12–14]. However, due to its heat transfer characteristics, the packed-bed operation may lead to hot-spot formations in case of highly exothermic reactions, as also shown in Fig. 2. Therefore, use of microchannel geometry rather than a packed-bed scheme can bring robustness against catalyst deactivation by hot spot driven thermal sintering [15].

Dynamic analysis of the microchannel operation requires the inclusion of time as a variable to the model equations ((4)–(10)). This leads to a partial differential equation set with three independent variables (t, ξ, z). However, if the same analysis is performed using the one-dimensional model, the cost of mathematical solution will be significantly lower due to the presence of two independent variables in the resulting PDE set (t, z). Comparison of the steady-state results shows that both models give close responses, and the differences in product yields of two models are mainly due to the temperature sensitivity of the rate expression used to describe methane steam reforming. Therefore, the one-dimensional pseudohomogeneous tubular reactor model can be used in making approximate but descriptive analysis of a wall-coated microchannel at a significantly reduced cost of formulation and solution. Similar studies using the one-dimensional model for analyzing the kinetics of a first order heterogeneous reaction running over the walls of a tube have been reported [15,16].

The model equations used to analyze the transient characteristics of the wall-coated microchannel are given in Section 2.2. Simulation results for the start-up of indirect partial oxidation subject to different initial and boundary conditions (Table 4) show that temperature increase in the axial direction is monotonic, and is consistent with the results obtained from the steady-state simulations (Fig. 3). Likewise, temporal increase in temperature at every point of the reactor is observed until steady state is reached. The duration of transient operation is between 100 and 120 s (Fig. 3). Note that the temperature profile of Run 1 is given as the representative result in Fig. 3, since Runs 1–3 are found to exhibit similar trends.

The steady-state product and exit temperatures at each run, predicted by steady-state and dynamic simulations are presented in Table 7. The deviations between two simulation

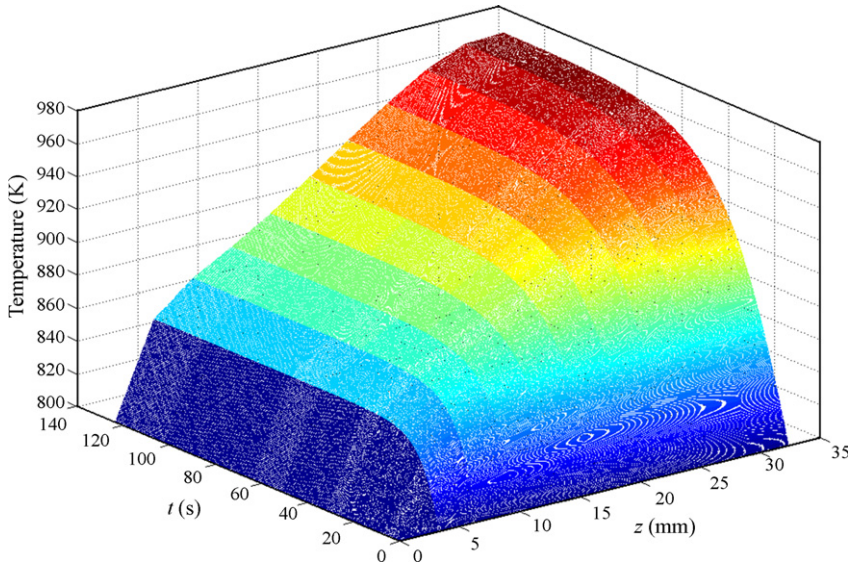

Fig. 3. Temperature variation in the microchannel as a function of time and axial distance ($CH_4/O_2 = 2.24$ and $H_2O/CH_4 = 1.17$).

types are small: the average of the percentage differences of three runs in the exit temperatures and methane conversions are 2.4% and 8.1%, respectively. These differences are mainly attributed to the approximations introduced by the numerical method used for solving the set of partial differential equations ((17)–(20)) [19,20]. Deviations in the product yields, on the other hand, are more significant and are equal to 21.8% for hydrogen and 23.9% for carbon monoxide yields (based on average of the percentage differences of three runs) (Table 7). Temperature sensitivity of the rate expression used to quantify methane steam reforming kinetics, which was mentioned above, seem to have a role in these higher deviations. Both simulation types predict the magnitudes of the exit temperatures in the order of Run 2 > Run 3 > Run 1. In Run 2, a temperature difference of 12.5 K leading to 1081.9 K results in increases of 32% and 36% in H_2 and CO yields, respectively (Table 7). In Run 3, where the dynamic simulation predicts a 4% higher exit temperature of 1066.3 K, increases in H_2 and CO yields are limited to 24.8% and 26.8%, respectively. In Run 1, where the exit temperature is predicted to be below 1000 K, both of the product yields seem to deviate only by ca. 8.7%. These results clearly show that, even though their deviations are small, the higher the magnitudes of the exit temperatures, the more the product yields from steady and dynamic simulations deviate. Such a trend indicates the dominance of temperature response of methane steam reforming. Apart from their quantitative similarity, both simulation types give similar qualitative responses. The results obtained by dynamic simulations conform to the trend that a decrease in the methane-to-oxygen ratio leads to higher temperatures, which in turn increases the hydrogen yield (Runs 1 and 2 in Table 7). Also, at constant methane-to-oxygen ratio, an increase in the steam flow rate lowers the bed temperature (Runs 2 and 3 in Table 7). Although catalytic operation is not expected to be adversely affected at these conditions, the exit temperature in Run 2 is critically high, which, in case of a disturbance, may begin increasing indefinitely (run-away situation), hence the catalyst may become prone to sintering.

In addition to the analysis of reactor start-up, responses of the microchannel, which is initially at steady state, to a set of disturbances in the feed, i.e. changes in methane-to-oxygen and steam-to-methane ratios, are also investigated. In case of a disturbance that involves a decrease in the methane-to-oxygen ratio from 2.24 to 1.89, more methane is combusted as a result of increased flow rate of air (Tables 5 and 8). This eventually leads to elevation of the temperature as illustrated in Fig. 4. Before the disturbance, the highest temperature attained by the partial oxidation process at steady state is 978 K, which, upon the change in the feed condition increases to its new steady-state value of 1073 K within a time period of ca. 90 s. Temperature increase leads to the generation of more exothermal heat, which is then utilized by the endothermic

Table 7
Comparison of steady methane conversions, product yields and temperatures obtained from steady-state and dynamic simulations

Run	Steady-state simulation				Dynamic simulation			
	x_{CH_4}	y_{H_2}	y_{CO}	T_{exit} (K)	x_{CH_4}	y_{H_2}	y_{CO}	T_{exit} (K)
1	82.60	202.06	44.91	998.56	71.37	219.66	48.86	978.53
2	95.60	225.80	53.71	1069.44	88.80	297.86	73.04	1081.87
3	86.02	203.25	46.00	1024.82	82.82	253.66	58.33	1066.28

Table 8
Methane conversion, product yields and exit temperatures at subsequent steady states

Case	Before disturbance				After disturbance			
	x_{CH_4}	y_{H_2}	y_{CO}	T_{exit} (K)	x_{CH_4}	y_{H_2}	y_{CO}	T_{exit} (K)
1	71.37	219.66	48.86	978.53	87.90	291.70	70.95	1073.07
2	88.80	297.86	73.04	1081.87	85.34	272.37	64.53	1065.02

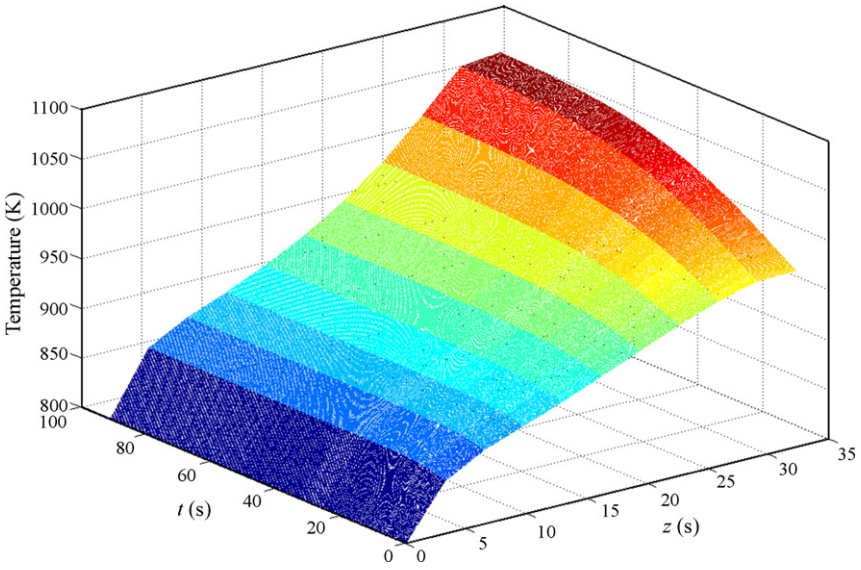

Fig. 4. Variation of temperature upon the decrease in CH_4/O_2 from 2.24 to 1.89.

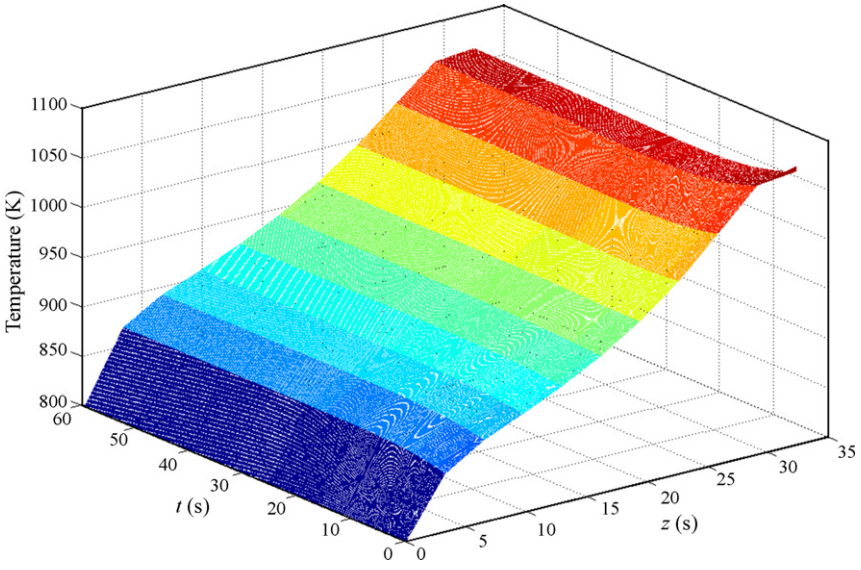

Fig. 5. Variation of temperature upon the increase in H_2O/CH_4 from 1.17 to 1.56.

steam reforming, resulting in 33% increase in hydrogen and 45% increase in carbon monoxide yields, respectively (Case 1, Table 8). Increase in methane conversion is both due to higher total oxidation and steam reforming conversions achieved.

In contrast with the temperature increasing effect of air addition, increase in the steam flow rate, as verified by steady-state and start-up simulations, lowers the reactor temperature (Tables 6 and 7). The same behavior is expected when this addition is made by way of a disturbance that alters the H_2O/CH_4 feed ratio of the reaction system, that is initially at steady state. Fig. 5 shows that when the inlet steam-to-methane ratio is increased from 1.17 to 1.56 (Table 5), at the same time keeping the amount of methane constant, a temporal temperature decrease is observed for about 10 s until a minimum is encountered, in this case corresponding to 1059 K. After 10 s the temperature begins to rise and settles to the steady-state value of 1065 K in 50 s.

The rates of steam reforming reactions are accountable for the inverse response realized in Fig. 5. Steam reforming is favored at high temperatures, however, upon increasing the steam flow rate, the temperature, hence the reforming rate is lowered. While reforming, which can be considered as a heat sink, heat released by the exothermic total oxidation raises the temperature. Since there is no other exogenous disturbance involved, increase in temperature and product yields is observed until the subsequent steady state is reached with decreases of 9% and 12% in hydrogen and carbon monoxide yields, respectively (Case 2, Table 8).

4. Conclusions

Mathematical models have been developed for simulating the steady and dynamic behaviors of a wall-coated catalytic microchannel in which hydrogen is produced from methane by

an indirect partial oxidation mechanism. The system is modeled at steady state using a two-dimensional axisymmetric wall-coated reactor model and a one-dimensional pseudohomogeneous tubular reactor model. The latter has the advantages of easier formulation and solution and has been proposed due to small channel diameter, adiabatic operating conditions and minimized transport resistances, all of which allow the system to be considered as a pseudohomogeneous entity having significant gradients only in the axial direction. Qualitative and quantitative results of the simulations, carried out for feed ratio ranges of $1.89 < CH_4/O_2 < 2.24$ and $1.17 < H_2O/CH_4 < 2.34$ for both models, are found to be close to each other; average difference between the simulated maximum bed temperatures are within 2%. Differences in product yields – 25% for hydrogen and 10% for carbon monoxide – are mainly due to the temperature sensitivity of the rate expression used to describe methane steam reforming kinetics. Based on these observations, numerical analysis of the transients of the microchannel operation is conducted using the lower cost one-dimensional model. The unsteady state (dynamic) one-dimensional model is then solved to characterize start up of the IPOX operation at three different combinations of feed ratios. The period between the start up and steady state of the microchannel is found to be between 100 and 120 s depending on the feed ratio. When compared with its steady-state counterpart, the dynamic model gave somewhat higher estimates for the steady-state parameters, which is mainly due to the approximation introduced by the finite difference method used to solve partial differential equations coupled with the temperature response of steam reforming kinetics. The series of analyses investigating the dynamic responses of the microchannel operating at steady state against disturbances in the feed composition showed that it took ca. 90 s for the system to reach its new steady state having ca. 100 K of higher exit temperature and 33% of higher hydrogen yield, when methane-to-oxygen ratio is reduced from 2.24 to 1.89. A temporal temperature decrease from 1082 K and a 9% reduction in hydrogen yield have been the responses to an increase in the steam flow rate, changing the steam-to-methane ratio from 1.17 to 1.56. In 10 s a minimum of 1059 K has been encountered, but due to the dominant exothermic oxidation reaction at this minimum, temperature has begun rising and then settled down to 1065 K in 50 s. Higher CH_4/O_2 (=2.24) ratios generate heat to drive steam reforming only at lower rates, whereas increased quantities of steam, dictated by elevated H_2O/CH_4 ratios (=2.34), inhibit steam reforming and reduce the amount of hydrogen generated. Therefore the feed composition of $CH_4/O_2 = 1.89$ and $H_2O/CH_4 = 1.17$ is found to be optimum in terms of maximum methane conversion and highest hydrogen yield.

Acknowledgments

The financial support for this research has been provided by TÜBİTAK-MAG through project 104M163 and Boğaziçi University Research Fund through projects DPT-03K120250 and BAP-06A503. A.E. Aksoylu acknowledges TUBA-GEBIP program.

References

[1] T.R. Ralph, G.A. Hards, Chem. Ind. 9 (1998) 337.
[2] S. Ahmed, M. Krumpelt, Int. J. Hydrogen Energy 26 (2001) 291.
[3] C. Song, Catal. Today 77 (2002) 17.
[4] A. Qi, B. Peppley, K. Karan, Fuel Process. Technol. 88 (2007) 3.
[5] T.R. Ralph, Platinum Metals Rev. 43 (1999) 14.
[6] D.L. Trimm, Z.İ. Önsan, Catal. Rev. Sci. Eng. 43 (2001) 31.
[7] A.K. Avcı, D.L. Trimm, Z.İ. Önsan, Chem. Eng. J. 90 (2002) 77.
[8] A.K. Avcı, Z.İ. Önsan, D.L. Trimm, Appl. Catal. A: Gen. 216 (2001) 243.
[9] L.F. Brown, Int. J. Hydrogen Energy 26 (2001) 381.
[10] L. Ma, D.L. Trimm, Appl. Catal. A: Gen. 138 (1996) 265.
[11] A.K. Avcı, D.L. Trimm, A.E. Aksoylu, Z.İ. Önsan, Catal. Lett. 88 (2003) 17.
[12] L. Kiwi-Minsker, A. Renken, Catal. Today 110 (2005) 2.
[13] G. Kolb, V. Hessel, Chem. Eng. J. 98 (2004) 1.
[14] C. Cao, Y. Wang, R.T. Rozmiarek, Catal. Today 110 (2005) 92.
[15] V. Hessel, S. Hardt, H. Löwe, Chemical Micro Process Engineering: Fundamentals, Modelling and Reactions, Wiley-VCH, Weinheim, 2004, p. 125.
[16] J.M. Commenge, L. Falk, J.P. Corriou, M. Matlosz, in: Proceedings of the 5th International Conference on Microreaction Technology, Strasbourg, May 27–30, (2001), p. 131.
[17] L. Ma, D.L. Trimm, C. Jiang, Appl. Catal. A: Gen. 138 (1996) 275.
[18] T. Numaguchi, K. Kikuchi, Chem. Eng. Sci. 43 (1988) 2295.
[19] J.C. Strikwerda, Finite Difference Schemes and Partial Differential Equations, Wadsworth & Brooks/Cole, California, 1989, p. 32.
[20] R.J. LeVeque, Finite Volume Methods for Hyperbolic Problems, Cambridge University Press, Cambridge, 2002, p. 68.
[21] B.S. Çağlayan, A.K. Avcı, Z.İ. Önsan, A.E. Aksoylu, Appl. Catal. A: Gen. 280 (2005) 181.
[22] J.R. Rostrup-Nielsen, in: J.R. Anderson, M. Boudart (Eds.), Catalysis, Science and Technology, vol. 5, Springer, Berlin, 1984, p. 3.